Cell Chemical Biology, Volume *24*

Supplemental Information

Directed Evolution of a Bright Near-Infrared Fluorescent Rhodopsin Using a Synthetic Chromophore

Lukas Herwig, Austin J. Rice, Claire N. Bedbrook, Ruijie K. Zhang, Antti Lignell, Jackson K.B. Cahn, Hans Renata, Sheel C. Dodani, Inha Cho, Long Cai, Viviana Gradinaru, and Frances H. Arnold

Supplemental Information

Supplemental Figures

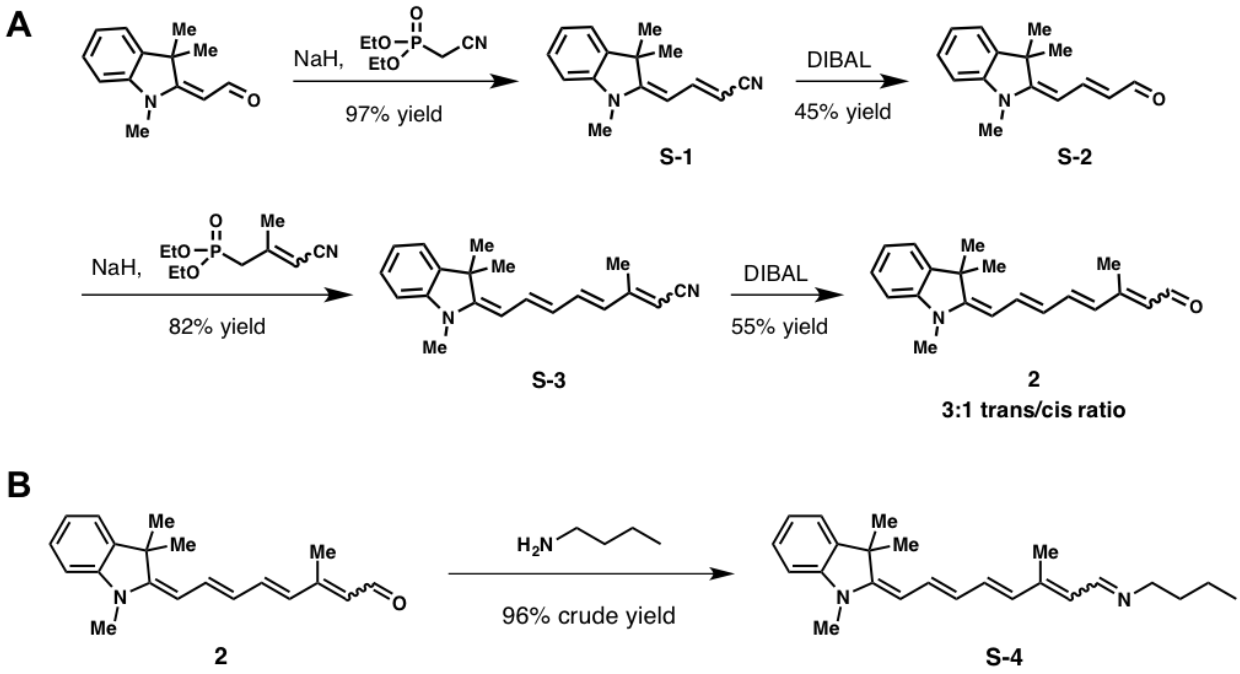

Figure S1. Synthesis of merocyanine retinal and subsequent synthesis of Schiff base. Related to Figure 1. (A) Merocyanine retinal was synthesized as shown above. Full characterization of the final compounds can be found at the end of this document. The final aldehyde product yielded a 3:1 *trans*:*cis* ratio at C16 (wavy line). This final aldehyde product is used throughout this work, and concentration values represent the total merocyanine retinal concentration (both trans and 16-*cis*). (B) The aldehyde form of merocyanine retinal was converted to a free Schiff base as described in the supplemental experimental procedures.

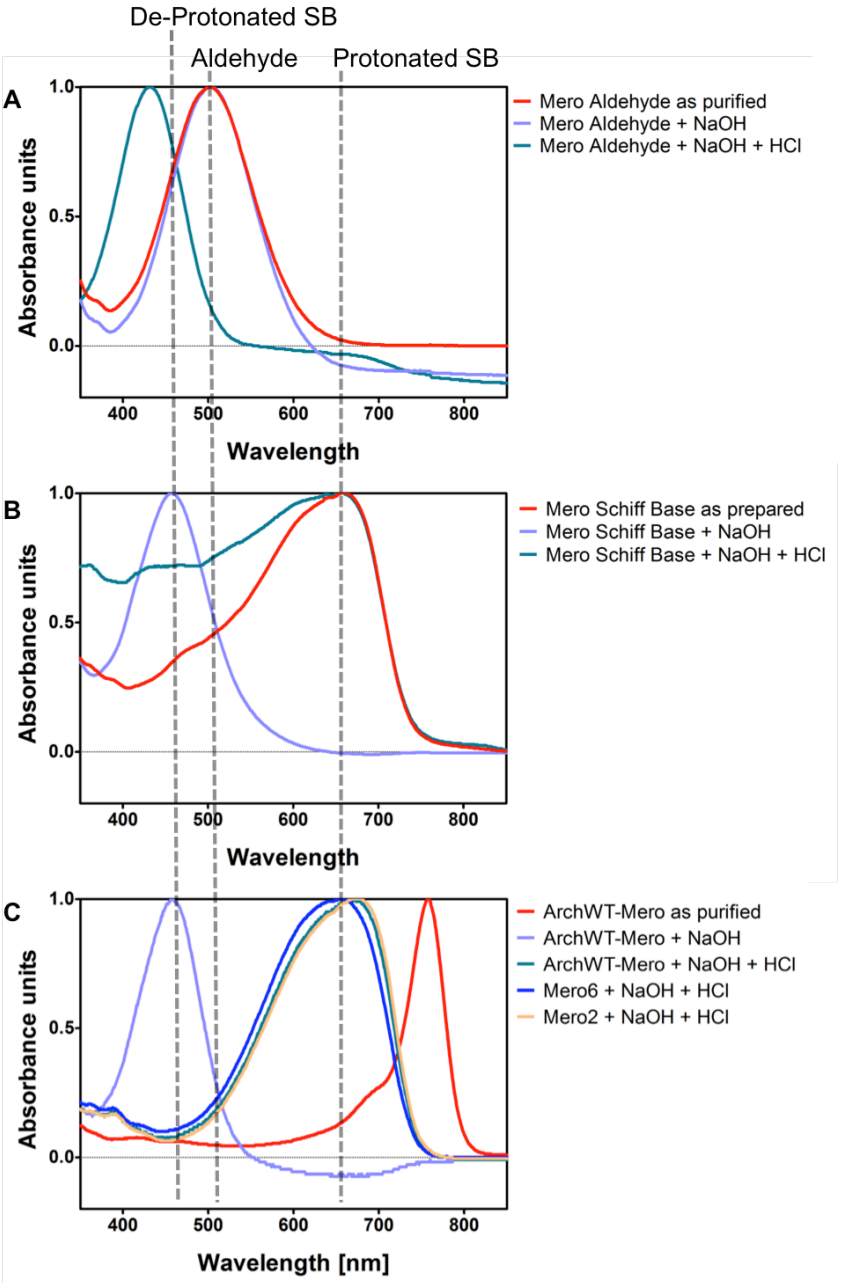

Figure S2. Base denaturation of merocyanine-bound Arch variants and free merocyanine retinal controls. Related to Figure 1. (A) Normalized absorbance spectra of the aldehyde form of merocyanine retinal (Mero) as purified (red), in alkaline conditions (light blue), and in acidic conditions (green). The acid peak at 435 nm likely represents protonated indolylidene ring. (B) Normalized absorbance spectra of the Schiff base (SB) form of merocyanine retinal prepared in crude reaction (red), in alkaline conditions (light blue), and in acidic conditions (green). Synthesis and characterization of the SB product are described at the end of this document. Over the course of minutes, the protonated Schiff base peak diminished and a protonated indolylidene ring peak formed at 435 nm; for clarity, only an early time point (within 1 min of adding acid) is shown, with its distinct yet incompletely formed protonated Schiff base peak. (C) Normalized absorbance spectra of purified wild-type Arch bound to merocyanine (red). Base denaturation yields a deprotonated Schiff base peak (light blue). Subsequent addition of acid yields a broad protonated Schiff base peak (green). Similar results were observed for Mero2 and Mero6 with the protonated Schiff base spectra shown in orange and dark blue, respectively. All measurements were taken in buffer [25 mM Tris; pH 6.5; 200 mM NaCl; 0.15% DDM] with serial reads taken after base denaturation (20 µL 5.6M NaOH added

to 600 µL sample), then acidification (40 µL 5M HCl added to 620 µL sample). Less base (5 µL) and acid (10 µL) were added to the free-Schiff base control due to a tendency to form protonated indolylidene in the acidic spectrum. Spectra were normalized to a maximal peak value of 1.

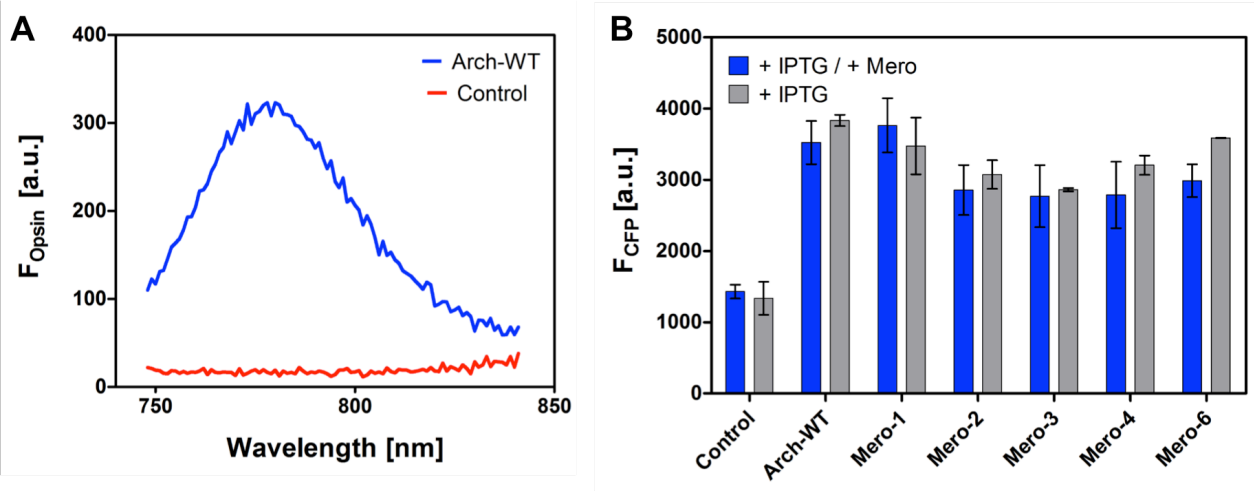

Figure S3. Merocyanine retinal specific opsin fluorescence in *E. coli* and the effect of merocyanine retinal on expression of Arch variants. Related to Figure 2. (A) Blue curve: Emission spectrum of Arch-WT (wild-type Arch); red curve: ScADH6 (*Saccharomyces cerevisiae* cinnamyl alcohol dehydrogenase); both spectra were recorded upon 720 nm excitation using a Tecan Infinite® M200 plate-reader; proteins were expressed in presence of 1 µM merocyanine retinal and 500 µM IPTG. ATR-bound Arch-WT excites and emits at 556/687 nm (McIsaac et al., 2014). (B) Expression is quantified by the fluorescence intensity of a C-terminally fused CFP tag (ex/em at 425/475 nm). CFP florescence measurements are taken on IPTG-induced *E. coli* suspensions in the presence (blue bars) and the absence (grey bars) of 10 µM merocyanine retinal (Mero). For all tested variants, merocyanine retinal has an insignificant effect on CFP fluorescence. A 10-fold greater concentration of merocyanine retinal was used in this test, but all other factors are identical to screening conditions (e.g. 500 µM IPTG). Error bars represent the standard deviation of six (with merocyanine) or two measurements (without merocyanine). The control protein (ScADH6 (*Saccharomyces cerevisiae* cinnamyl alcohol dehydrogenase)) does not encode CFP and represents the nonspecific cellular background signal.

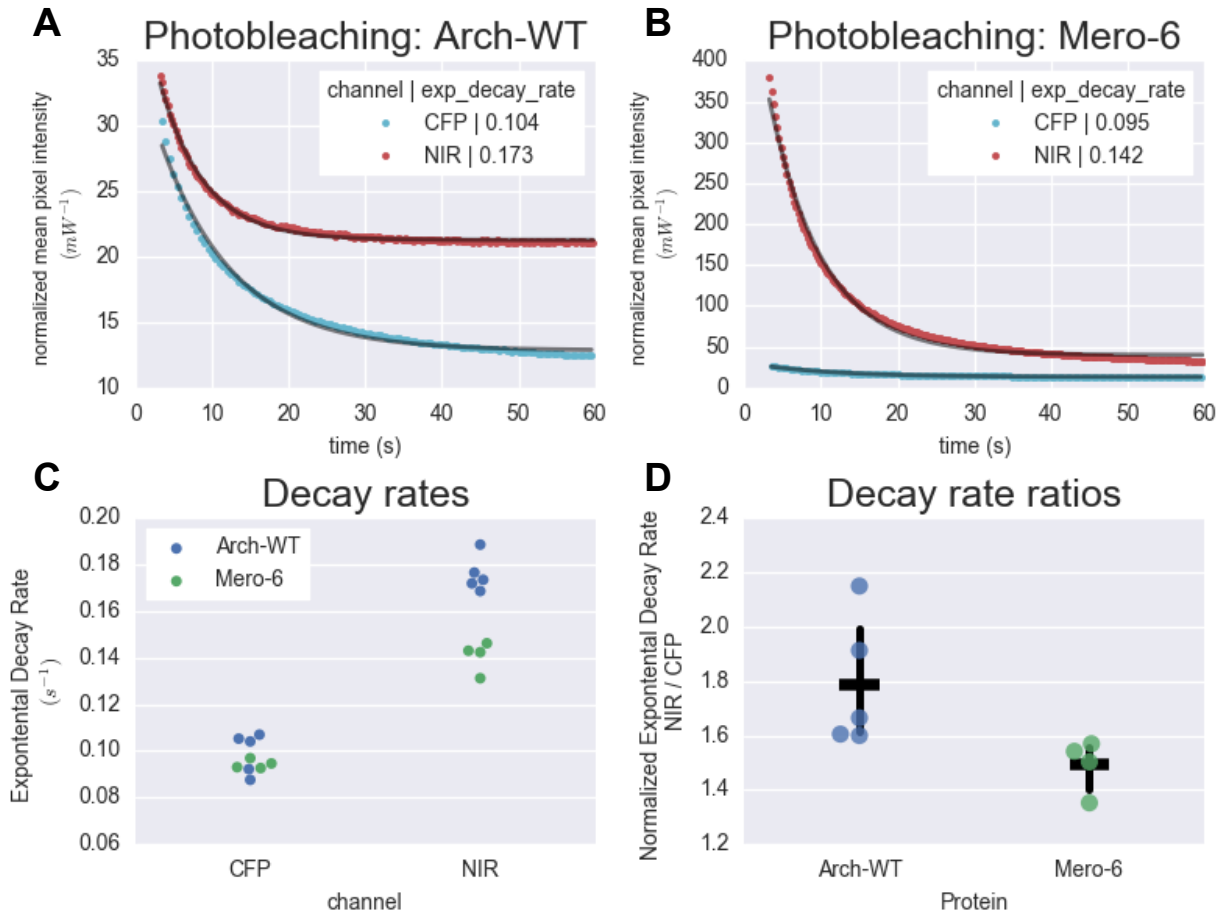

Figure S4. NIR photo-bleaching of merocyanine-bound Arch variants in *E. coli*. Related to Figure 4. Representative decay curves of CFP-tagged Arch-WT (A) and Mero-6 (B). Each *E. coli* image contained multiple *E. coli* cells within the field of view. For each *E. coli* image, CFP and Arch fluorescence were respectively bleached with 405 nm light (500 ms exposures; teal dots) then near-infrared (NIR) 727 nm light (250 ms exposures; red dots). Fluorescence was normalized for protein absorption profile and laser power. Each decay curve was fit with a single exponential curve (black) between 3 and 60 seconds. The decay rates for the representative curves are shown in the legends (units = s^{-1}). (C) Decay rates determined for CFP-tagged Arch-WT (n = 5 samples) and Mero-6 (n = 4 samples), in both the CFP and NIR channels. (D) For each sample of Arch-WT (blue dots) and Mero-6 (green dots), the decay rate of merocyanine-bound Arch (determined in the NIR channel; 727 nm) was normalized by the decay rate of CFP (determined at 405 nm). The black horizontal line marks the mean normalized decay rate (Table 1) and the black vertical bars represent the 95% confidence interval determined from 1000 bootstraps.

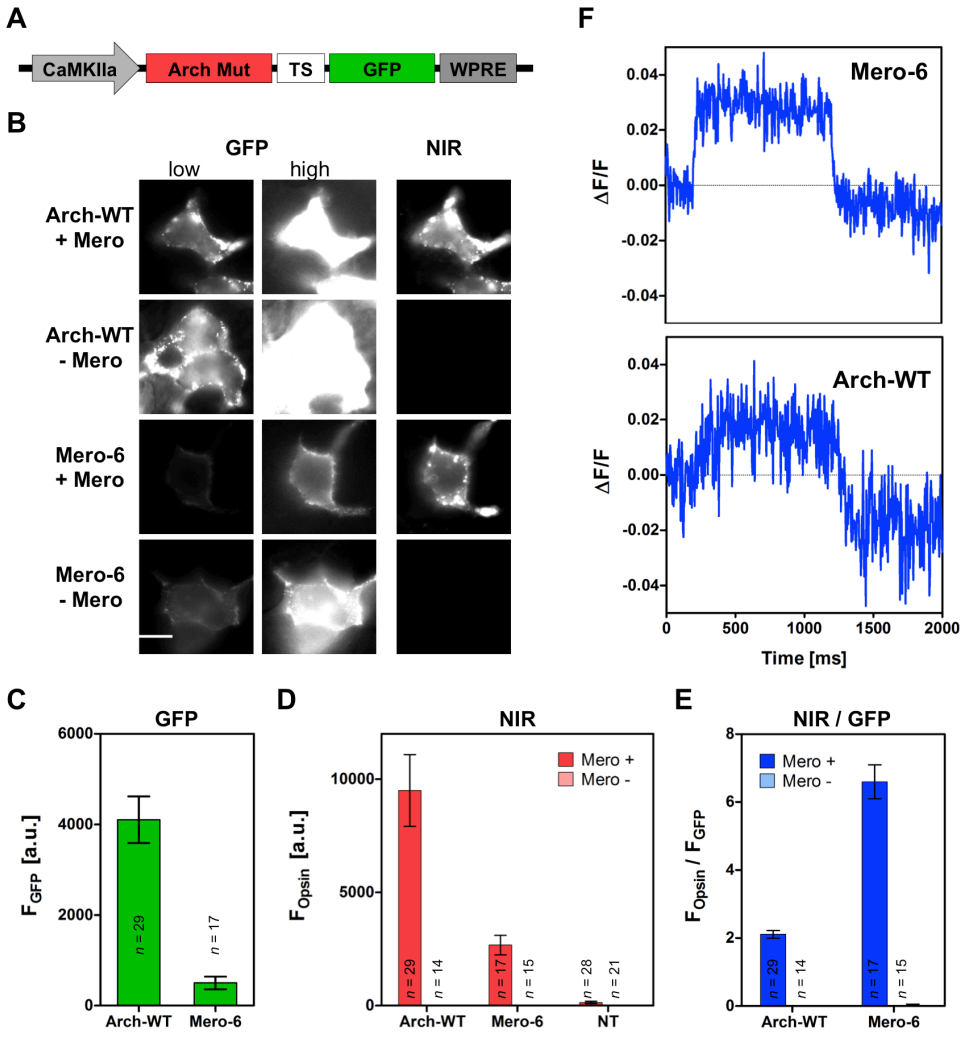

Figure S5. Expression and NIR fluorescence in live eukaryotic (HEK) cells grown in D10 medium. Related to Figure 4. (A) Eukaryotic construct for expression of a fusion of GFP and Arch mutant (Arch Mut) driven by a CaMKIIa promoter. TS: trafficking sequence. ES: Export signal. WPRE: woodchuck hepatitis virus post-transcriptional enhancer. (B) Representative NIR (ex/em 727/766-854 nm) and GFP (ex/em 473/>498 nm) fluorescence images of HEK cells expressing wild-type Arch or Mero-6. Low and high contrast images of the GFP channel are shown due to significant differences in expression between Arch variants; such treatment was not required in the NIR channel due to enhanced fluorescence intensity of Mero-6. Indicated HEK cells are expressed with merocyanine retinal (1 µM final concentration) for 24 hrs. Scale bar: 10 µm. (C) Mean GFP fluorescence intensity of HEK cells expressing Arch-WT (n = 29) and Mero-6 (n = 17). (D) Mean NIR fluorescence of WT, Mero-6, and non-transfected (NT) cells with merocyanine (n = 29, 17, and 28, respectively) and without merocyanine (n = 14, 15, and 21 respectively). (E) NIR fluorescence normalized by GFP fluorescence for HEK cells with or without merocyanine added. All error bars represent one standard error of the mean. (F) Patch-clamp electrophysiology of transfected HEK cells was used to test merocyanine retinal-bound, wild-type Arch (n = 7 cells) and Mero-6 (n = 10 cells) for voltage sensitivity. Both variants were expressed in the presence of 1 µM merocyanine retinal for 24 hrs. With excitation at 650 nm and detection >780 nm, wild-type Arch showed approximately 2% change in fluorescence intensity during a 100 mV step in the clamped voltage (voltage step from -70 mV to +30 mV). However, precise measurement of the intensity change is difficult due to high noise levels in the wild type readings. Mero-6 readings were less noisy and showed a 4% change in fluorescence intensity with an identical voltage step. ΔF/F = change in fluorescence from baseline, normalized by baseline fluorescence.

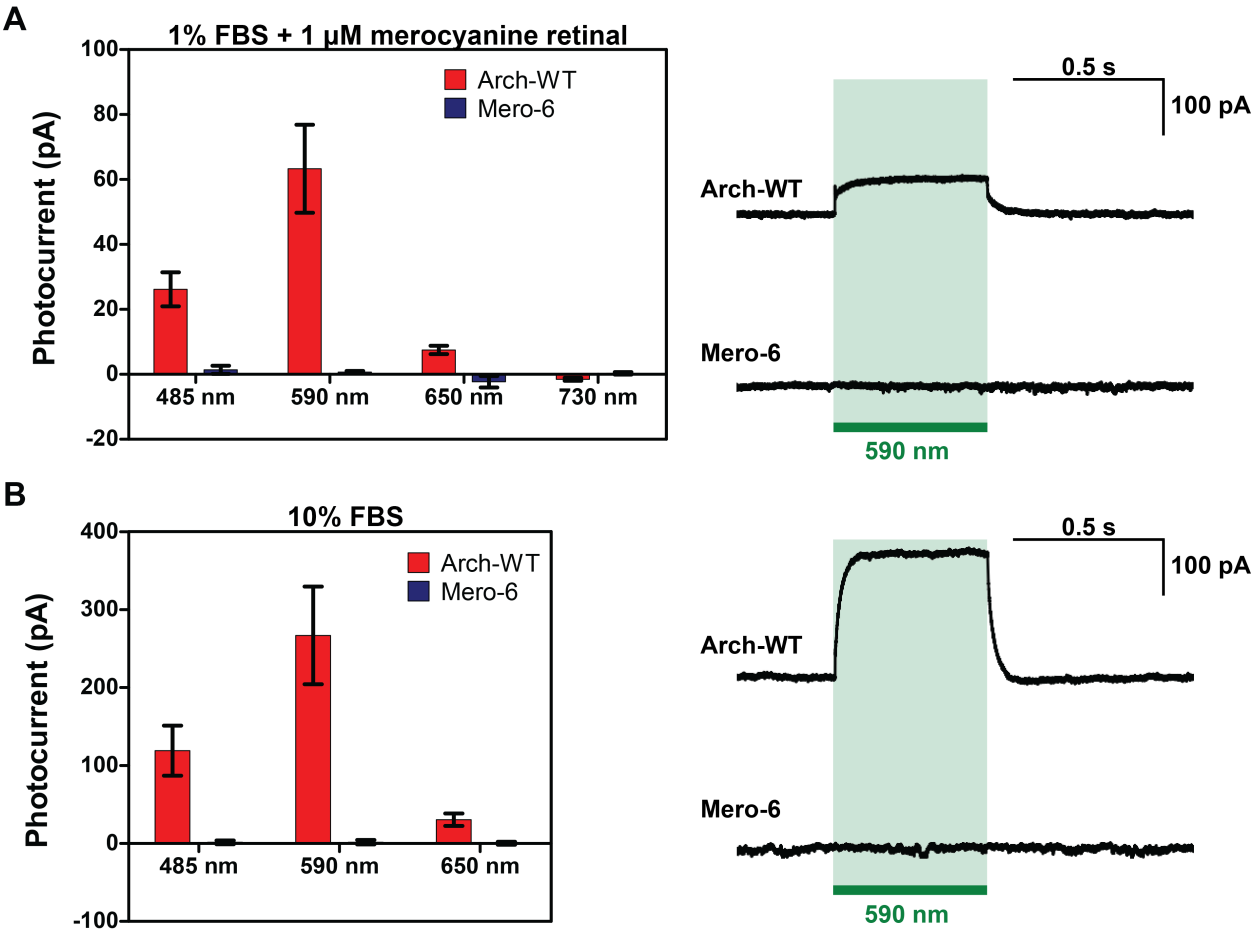

Figure S6. Light-driven ion pumping in HEK cells. Related to Figure S5. Patch-clamp electrophysiology of transfected HEK cells was used to measure photocurrents of wild-type Arch and Mero-6 with short light pulses (0.5 s) of varying wavelength. Recordings were done of cells incubated with media containing (A) 1% FBS with 1 µM merocyanine retinal added or (B) 10% FBS without any added merocyanine retinal. The amount of FBS used dictates the concentration of ATR in the medium. Photocurrents were measured for four different wavelengths of light. Currents were only observed for wild-type Arch at 485 nm, 590 nm, and 650 nm but not 730 nm light with (n = 6 cells) or without (n = 10 cells) 1 uM merocyanine retinal. No currents were observed for Mero-6 at any wavelength with (n = 10 cells) or without (n = 7 cells) 1 µM merocyanine retinal. Example traces with 590 nm light for wild-type Arch and Mero-6 are shown to the left for both conditions (A) 1% FBS with 1 µM merocyanine retinal added and (B) 10% FBS. These results suggest that Mero-6 is incapable of pumping with either ATR or merocyanine retinal.

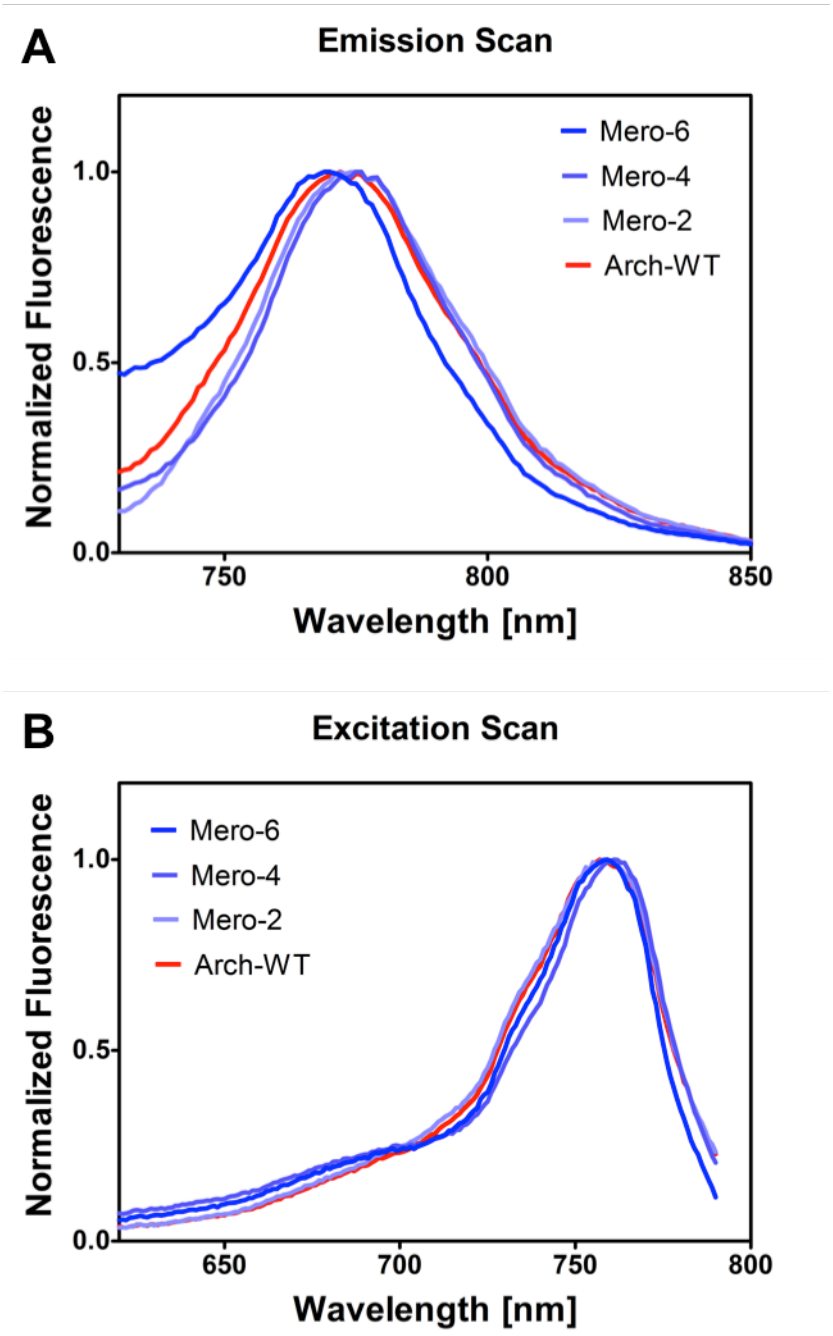

Figure S7. Spectral scans of purified merocyanine retinal-bound Arch variants. Related to Table 1. (A) Fluorescent emission scan (730-850 nm) with excitation set at 700 nm. (B) Excitation scan (610-790 nm) with emission detected at 810 nm. Spectra were collected from 200 μL samples (diluted with DDM desalt buffer to an absorbance (A_{680}) below 0.07) using a SpectraMax: M5 plate reader (4 nm bandwidth; 1 nm steps). Spectra were normalized to peak values.

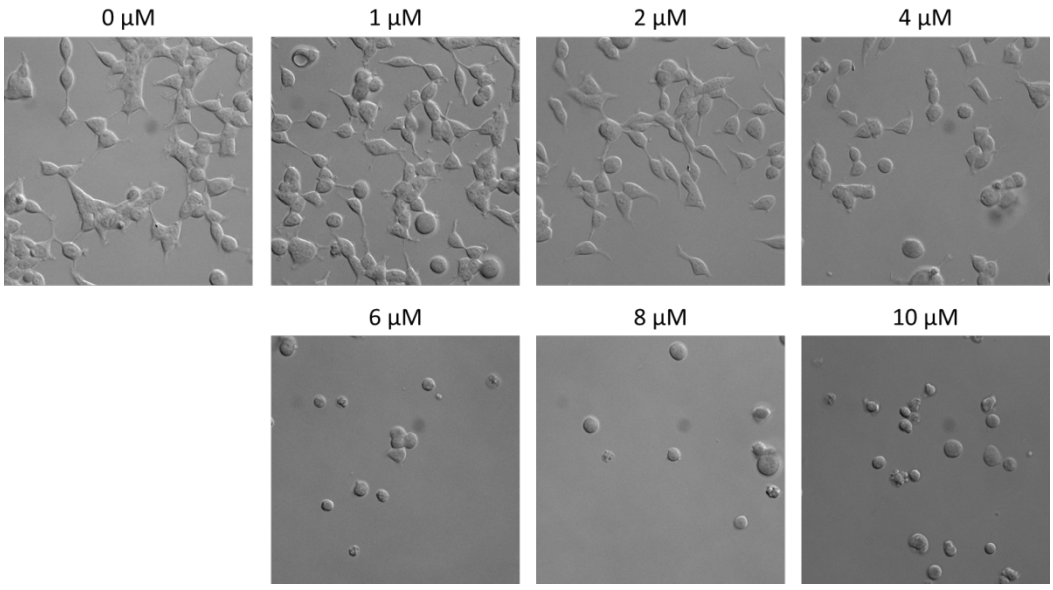

Figure S8. Effects of merocyanine retinal on HEK cell health. Related to Figure S5. Representative images of non-transfected HEK cells after a 48 hrs incubation with varying concentrations of merocyanine retinal (0-10 µM) in medium (DMEM with 1% FBS).

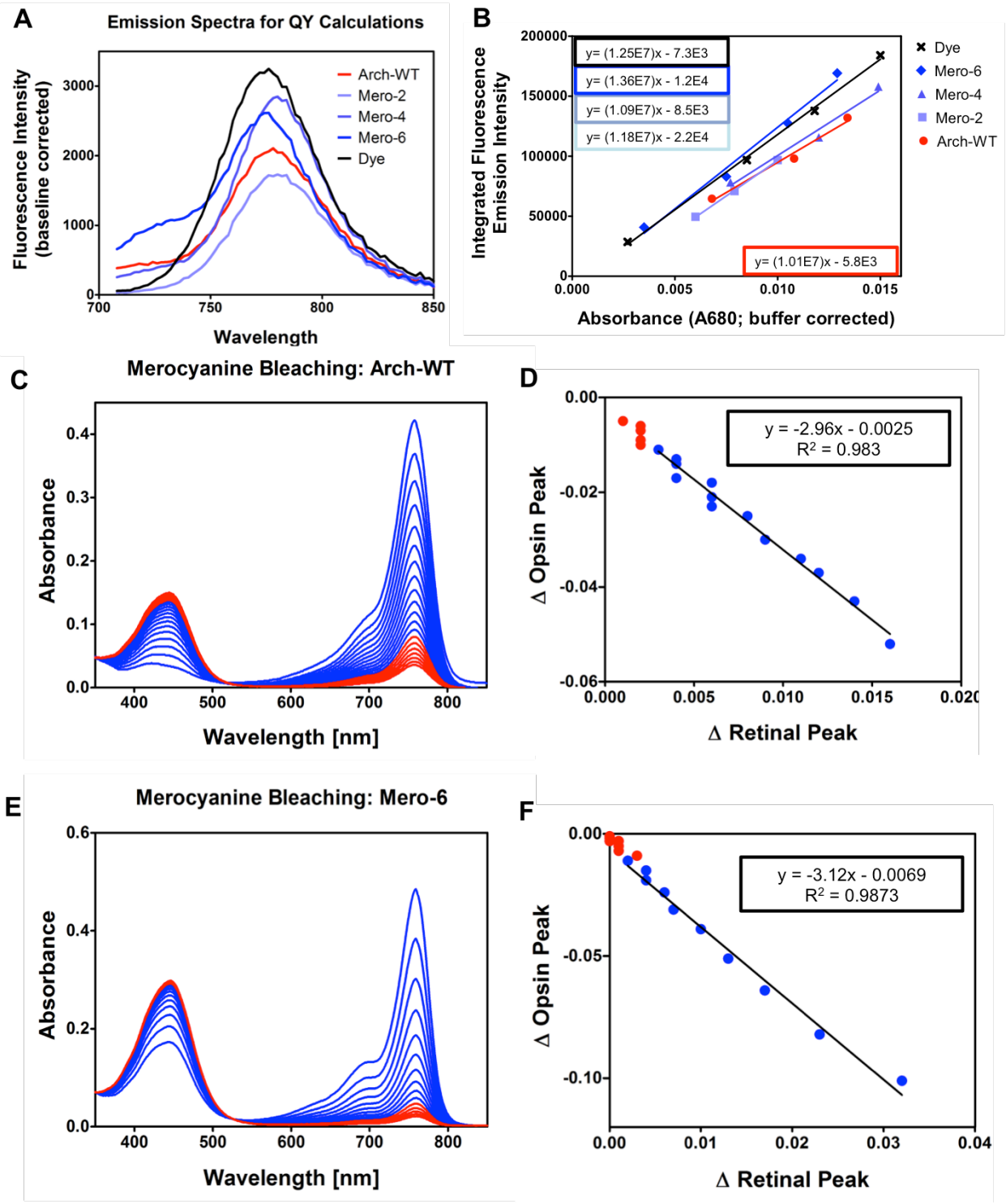

Figure S9. Representative data used in quantum yield and extinction coefficient calculations of merocyanine-bound Arch variants. Related to Table 1. (A) Representative fluorescent emission spectra (excitation at 680 nm) from one of four dilutions made for each Arch variant and standard dye (Alexa Fluor 750). Baseline fluorescence was measured for DDM desalt buffer (proteins) or PBS (dye). Spectra were integrated as described in methods. Absorbance values (A_{680}) were determined for each sample and dilution, which were corrected by buffer controls. (B) Plot of integrated fluorescence vs. absorbance. Equations are shown for linear regressions to each set of data. (C)

Time course of absorbance spectra (350-850 nm), collected during the hydroxylamine bleaching of merocyanine-bound Arch-WT every 12 min (C) and Mero-6 every 3 min (E). Peak values of pigmented opsin (758-761 nm depending on mutant) and the free oxime form of retinal (441 nm) were monitored. The change in absorbance over time for pigmented opsin protein (ΔOpsin) is plotted against the concurrent change in oxime retinal for Arch-WT (D) and Mero-6 (F). The linear region of the plot (blue spectra in C and E contributing blue points in D and F) is fitted with a linear regression (equation and R^2, shown). Data points with minimal change in oxime retinal absorption (red points from red spectra) were excluded from the regression. The slope of the linear regression (ΔOpsin / ΔRetinal) was used in determining the extinction coefficient for each variant (see Supplemental Experimental Procedures).

Supplemental Data

Data S1. NMR characterization of merocyanine retinal synthesis. Related to experimental methods and Figure S1. NMR spectra are shown with the structure of corresponding intermediate and target compounds. To help interpret the ^{1}H NOESY experiments, circled peaks are paired with indicated interactions via color-coding.

Supplemental Experimental Procedures

Arch-His_{6x} and Arch-CFP Nucleotide Sequences

> Arch-His_6

ATGGACCCGATTGCTCTGCAGGCAGGTTACGACCTGCTGGGTGATGGCCGTCCGGAAACCCTGTGGCT
GGGTATTGGTACCCTGCTGATGCTGATCGGCACCTTCTACTTCCTGGTGCGTGGCTGGGGCGTCACTGA
TAAGGATGCTCGTGAATACTACGCTGTTACCATCCTGGTGCCAGGCATTGCGAGCGCAGCTTACCTGT
CTATGTTCTTCGGCATCGGTCTGACCGAAGTAACGGTAGGTGGTGAAATGCTGGACATTTACTACGCA
CGTTACGCTGACTGGCTGTTCACTACCCCACTGCTGCTGCTGGATCTGGCTCTGCTGGCCAAAGTTGAC
CGTGTTACCATCGGCACTCTGGTAGGTGTGGACGCACTGATGATCGTGACCGGTCTGATTGGTGCTCT
GTCTCACACTGCTATCGCTCGTTATTCCTGGTGGCTGTTTAGCACCATCTGCATGATTGTGGTGCTGTA
CTTCCTGGCGACCTCTCTGCGCTCCGCTGCTAAAGAGCGTGGTCCGGAAGTTGCTTCTACTTTTAACAC
CCTGACCGCTCTGGTGCTGGTGCTGTGGACCGCTTATCCTATCCTGTGGATCATCGGCACCGAAGGTG
CGGGTGTTGTTGGTCTGGGCATTGAAACCCTGCTGTTCATGGTTCTGGATGTTACTGCCAAAGTTGGCT
TTGGTTTTATTCTGCTGCGTTCCCGTGCGATCCTGGGTGACACCGAAGCCCCAGAACCGAGCGCTGGT
GCAGATGTTTCCGCTGCGGACgcagctgcactcgagCACCACCACCACCACCACTGA

> Arch-eCFP

ATGGACCCGATAGCACTACAGGCGGGATACGACCTACTCGGGGACGGTCGCCCCGAGACGTTGTGGT
TGGGTATCGGAACGTTACTAATGCTCATCGGGACCTTCTACTTCCTCGTCAGAGGGTGGGGGGTCACC
GACAAGGACGCCCGCGAGTACTACGCGGTCACGATCCTCGTGCCGGGGATCGCGTCGGCGGCGTACC
TGTCGATGTTCTTCGGCATCGGCCTGACGGAAGTCACGGTCGGTGGCGAAATGCTCGACATCTACTAC
GCGCGGTACGCGGACTGGCTGTTCACCACGCCGCTGCTGCTGCTCGACCTCGCGCTGCTCGCAAAGGT
CGACCGCGTCACCATCGGGACGCTCGTCGGCGTCGACGCGCTGATGATCGTCACCGGCCTCATCGGCG
CGCTCTCGCACACGGCGATCGCGCGGTACTCCTGGTGGCTGTTCAGCACGATTTGCATGATCGTCGTG
CTGTACTTCCTCGCCACGAGCCTCCGGAGCGCGGCGAAGGAGCGCGGACCTGAAGTCGCGAGCACCT
TCAACACGTTGACCGCGCTGGTCCTGGTGCTCTGGACGGCCTACCCGATCCTGTGGATCATCGGAACC
GAGGGCGCCGGCGTCGTCGGCCTCGGCATCGAGACCCTCCTGTTCATGGTTCTCGACGTGACGGCCAA
GGTCGGCTTCGGCTTCATCCTGCTCCGCAGCCGCGCCATCCTCGGCGACACCGAGGCGCCGGAGCCCT
CCGCGGGCGCCGACGTCTCCGCCGCGGACgcggccgcactcgagATGGTGAGCAAGGGCGAGGAGCTGTTCA
CCGGGGTGGTGCCCATCCTGGTCGAGCTGGACGGCGACGTAAACGGCCACAAGTTCAGCGTGTCCGG
CGAGGGCGAGGGCGATGCCACCTACGGCAAGCTGACCCTGAAGTTCATCTGCACCACCGGCAAGCTG

CCCGTGCCCTGGCCCACCCTCGTGACCACCCTGACCTGGGGCGTGCAGTGCTTCAGCCGCTACCCCGA
CCACATGAAGCAGCACGACTTCTTCAAGTCCGCCATGCCCGAAGGCTACGTCCAGGAGCGCACCATCT
TCTTCAAGGACGACGGCAACTACAAGACCCGCGCCGAGGTGAAGTTCGAGGGCGACACCCTGGTGAA
CCGCATCGAGCTGAAGGGCATCGACTTCAAGGAGGACGGCAACATCCTGGGGCACAAGCTGGAGTAC
AACTACATCAGCCACAACGTCTATATCACCGCCGACAAGCAGAAGAACGGCATCAAGGCCAACTTCA
AGATCCGCCACAACATCGAGGACGGCAGCGTGCAGCTCGCCGACCACTACCAGCAGAACACCCCCAT
CGGCGACGGCCCCGTGCTGCTGCCCGACAACCACTACCTGAGCACCCAGTCCGCCCTGAGCAAAGAC
CCCAACGAGAAGCGCGATCACATGGTCCTGCTGGAGTTCGTGACCGCCGCCTAA

Purification of Arch variants

Arch variants of interest were transformed into NiCo-pLEMO cells and plated (LB; 100 µg/mL ampicillin; 34 µg/mL chloramphenicol) for lawn growth. The next day, cells were scraped from the plate, re-suspended in media (2xYT; 100 µg/mL ampicillin; 34 µg/mL chloramphenicol), and 1 mL of re-suspended cells inoculated into 1 L medium. For typical variants, at least 2 L of culture was prepared. Cultures were grown at 37 °C until an optical density of 0.6-0.8 was reached. At this point merocyanine retinal (at 10 mM in 100 % ethanol) and IPTG were added to a final concentration of 1 µM and 500 µM, respectively. Cells were then grown for 3 hours at 30 °C in the dark, harvested via centrifugation and stored at -80 °C.

Holo-Arch variants were purified as reported (McIsaac et al., 2014). Frozen cells were resuspended in buffer components such that the final solution consisted of [20 mM Tris-HCl; pH 7.5; 200 mM NaCl; 20 mM imidazole; 1% dodecylmaltopyranoside (DDM; Anatrace); 10 mg/mL lysozyme (Sigma); ~1 mg/mL DNase (Sigma)] with the final volume being ~5x the volume of the cells. Resuspended cells were incubated with shaking at room temperature in the dark for 1.5 hours, then centrifuged in a microcentrifuge for 30 min 4 °C. From this point on, the protein solution was kept on ice or at 4 °C and shielded from light. Variants were purified via nickel affinity chromatography (ÄKTA Express) wherein a 1 mL HisTrap HP column (GE healthcare) was equilibrated with [20 mM Tris-HCl; pH 7.5; 200 mM NaCl; 20mM imidazole; 0.02% DDM] then over-loaded with lysate. The loaded column was washed with 10 column volumes of equilibration buffer then eluted in a 20-500 mM imidazole gradient over 20 column volumes. Absorbance at 280 and 760 nm was monitored, and pigmented fractions with highest purity were pooled and immediately desalted into 'DDM desalt buffer' [20 mM Tris-HCl; pH 6.5; 200 mM NaCl; 0.15% DDM] via PD-10 desalting columns (GE Healthcare).

To prepare *apo* protein for retinal binding assays, Arch variants were expressed as described with retinal not added upon induction. To minimize temperature shock of what we expected to be a less stable *apo* protein, cells were lysed with a microfluidizer in the absence of detergent. Lysate was centrifuged at low speed (20,000 x g) to remove cell debris, then at high speed (185,500 x g) to collect membranes. Membranes were resuspended in [20 mM Tris-HCl; pH 7.5; 200 mM NaCl] and stored at -80 ˚C. Membranes were thawed on ice and dissolved with 1.5% lauryl maltose neopentyl glycol (LMNG) detergent. LMNG was found empirically to promote retinal binding to *apo*-Arch (wild-type *apo*-Arch could not bind ATR or merocyanine retinal if purified in DDM; data not shown). Dissolved *apo*-Arch membranes were purified via Ni affinity chromatography as described above except that 0.015% LMNG replaced DDM in all buffers, 4.5 mL of Ni-NTA superflow resin (Qiagen) was used, and protein was eluted in one step. SDS-PAGE confirmed the presence and purity of *apo* proteins before PD-10 desalting into [20 mM Tris-HCl; pH 7.5; 200 mM NaCl; 0.015% LMNG] ('LMNG desalt buffer'). For the binding assay, purified proteins were concentrated no more than 2x via spin filtration (Millipore).

Quantum yield and extinction coefficient determination

As described in Wall *et al*. (2015), the quantum yields of merocyanine-bound Arch variants were calculated by comparison of each variant to the Alexa Fluor® 750 NHS Ester (succinimidyl ester) dye with known quantum yield of 0.12 (catalog number: A20011, Life Technologies Corporation) (Wurth et al., 2012). With peak excitation/emission at 749/775 nm, this reference dye has similar spectral characteristics to the merocyanine-bound Arch variants. For each Arch variant and the reference dye, four serial dilutions were made with corrected absorbance values (A_{680}) below 0.04. For each dilution, a Tecan Infinite® M200 plate-reader was used to measure the A_{680}, then a fluorescence emission scan between 708-850 nm when excited at 680 nm (Figure S9*A*). The integrated fluorescence from each baseline-corrected emission peak was calculated via trapezoidal integration. Integrated fluorescence was plotted vs A_{680}; for each Arch variant and the reference dye, a slope (fluorescence/absorbance) was calculated (Figure S9*B*). These slopes (m) were used in the following equation to calculate the quantum yield of each protein (QY_P): $QY_P = QY_{ref} * (m_P / m_{ref}) * (\eta_P^2 / \eta_{ref}^2)$. Where η_P and η_{ref} are the respective refractive indices of the protein buffer [20 mM Tris-HCl; pH 6.5; 200 mM NaCl; 0.15% DDM] (η_P =

1.3359) and the dye buffer (PBS; η_{ref} = 1.3348) (refractometer model no. 334620; Fisher Scientific), and QY_{ref} is the quantum yield of the reference dye (QY_{ref} = 0.12; (Wurth et al., 2012)).

Similar methods were used to determine the quantum yield of the aldehyde form of merocyanine retinal in protein buffer. The standard dye Cy5.5 NHS ester (PA15601; GE healthcare) with the known quantum yield of 0.284 in PBS (Wurth et al., 2012) had excitation/emission wavelengths (673 / 707 nm) close enough to free merocyanine retinal (517 / 691 nm) for both to be detected with excitation at 540 nm and detection from 570 to 850 nm.

The extinction coefficient of each merocyanine-bound Arch variant was determined as described (McIsaac et al., 2014). Briefly, 117 µL of [2.7 M hydroxylamine; pH 6.7] was added to 517 µL diluted protein to give a final concentration of 0.5 M hydroxylamine (protein was diluted as necessary with DDM desalt buffer to give a peak absorbance of less than 1.0 OD in the final reaction mixture). Using a Shimadzu UV-1800 spectrophotometer (1 cm quartz cuvette), absorption spectra between 350 and 850 nm were collected every 3 to 12 min for 4 hours (Figure S9*C* and *E*). During the course of data collection no Arch variant visibly precipitated. The extinction coefficients ε_P were calculated according to the formula $\varepsilon_P = \varepsilon_R(\Delta A_P/\Delta A_R)$, where ε_R is the extinction coefficient of merocyanine retinal oxime, 26,226 $M^{-1}\cdot cm^{-1}$ (determined below), ΔA_P is the change in absorbance at the λ_{max} of Arch (which is different depending on the mutant) over time, and ΔA_R is the change in absorbance at 441 nm, from the formation of free merocyanine retinal oxime, over time. ($\Delta A_P/\Delta A_R$) was averaged over the linear portion of the hydroxylamine reaction for each mutant (Figure S9*D* and *F*). Since absorbance values are only taken from merocyanine-bound rhodopsin or freed retinal oxime, this bleaching method (for determining a rhodopsin extinction coefficient) avoids assumptions of protein purity or retinal occupancy that are inherent in methods requiring a dilution series of protein at known concentration.

The extinction coefficient of free merocyanine retinal oxime was determined from a dilution series of merocyanine retinal aldehyde. A known mass of merocyanine retinal was dissolved in ethanol to 2 mM and diluted 20x in DDM desalt buffer containing 0.5 M hydroxylamine. Subsequent samples in the dilution series were diluted by 66% in DDM desalt buffer containing 0.5 M hydroxylamine. Samples were kept shielded from light at room temperature for at least 4 hours to ensure complete conversion of the aldehyde to oxime. Conversion was verified by the shift in peak absorbance of free merocyanine retinal from 498 nm (aldehyde) to 441 nm (oxime). The clean and Gaussian absorbance peak suggests that the oxime form of merocyanine retinal is stable. Absorbance was plotted against [molar retinal concentration * 1 cm path length]; the slope of a linear regression ($r^2 > 0.99$) was the extinction coefficient. The average of three replicates was 26,226 M^{-1} cm^{-1} with a standard error of 2,007 M^{-1} cm^{-1}.

HEK cell maintenance and transfection

HEK 293T cells were cultured at 37 ^oC and 5% CO_2 in D10 (Dulbecco's modified Eagle medium (DMEM) supplemented with 10% (vol/vol) FBS, 1% sodium bicarbonate and 1% sodium pyruvate). 10% FBS contributes to a final concentration of approximately 30 nM ATR (Muenzner et al., 2013), which is comparable to the endogenous ATR concentration of rat brain tissue (Asson-Batres et al., 2009).

For imaging experiments HEK cells were seeded at low density into 96-well glass bottom plates with #1.5 cover glass with a poly-D-lysine coating. Cells were left to divide until they reached ~20-30% confluency. Wild-type Arch and variants were transfected into HEK cells with FuGENE6® according to the manufacturer's recommendations with one variant per well. The codon-optimize WT construct has been reported previously (Flytzanis et al., 2014); the codons for Mero-6 in HEK cell expression are based on this optimized WT protein. Twenty-four hours after transfection the D10 medium was replaced with D10 medium supplemented with 1 µM merocyanine retinal. Imaging was done 48 h post transfection. After this prolonged incubation, HEK cells were adherent with normal morphology and healthy appearance (Figure S8).

For electrophysiology experiments HEK cells were transfected with wild-type Arch and variants using FuGENE6® according to the manufacturer's protocol with 1 µM merocyanine retinal supplemented medium. Transfected HEK cells where then passaged and plated at a density of 5,000 cells per cm^2 onto 12 mm-poly-D-lysine coated coverslips at 16 h post-transfection. The HEK cells were left to adhere to coverslips and continue to express for another 30 h with 1 µM merocyanine retinal supplemented medium (total expression for 48 h post transfection).

***E. coli* and HEK cell imaging and data processing**

Two orthogonal channels (DAPI and Cy7 for *E. coli* or GFP and Cy7 for HEK) with laser illumination and corresponding filter cube sets were used for imaging on an inverted Olympus IX-81 microscope. The lasers lines for *E. coli* imaging 405 nm (Shanghai Dream Lasers Technology Co. Ltd, SDL-405-LM100T, measured power 111 mW) and 727 nm (Coherent CUBE, 1178855, measured power 32 mW) were used for excitation of the fluorophores with respective filter cubes used for detection at >418 nm (Semrock: LF405/LP-B-000) and 766-854 nm (Semrock:

Cy7-B-000). Likewise, the lasers for HEK imaging, 473 nm (CNI, MBL-FL-473, max power 100 mW) and 727 nm (Coherent CUBE, 1178855, measured power 32 mW) were used for excitation of the fluorophores with detection at >498 nm (Semrock: LF488/LP-C-000) and 766-854 nm (Semrock: Cy7-B-000). Two oil objectives, Olympus NA 1.40 UPlanSApo 100x with additional 1.6x magnification for *E. coli* and Olympus NA 1.35 UPlanSApo 60x for HEK cells were used for imaging. The camera was back-illuminated CCD Andor iKon-M 934 BEX2-DD, offering high quantum efficiency in the near infrared region with a pixel size of 13x13 μm. Open source Micro-Manager data acquisition software (v. 1.4.18) was used to run the microscope (Edelstein et al., 2010). Fluorescence analysis of E. coli clusters was done by masking the background in the CFP image (via an otsu threshold of pixel intensity counts) and determining the mean pixel intensity within the mask (signal) and outside the mask (background). The CFP signal was more consistent across variants so the CFP mask was applied to the NIR channel images (except for the non-opsin control, which had no CFP signal and was thus masked by the NIR signal). The background-corrected mean pixel intensities are reported in Figure 4*B-C*. The NIR/CFP ratio was determined for each cluster of cells and the ratios were averaged for the values given in Figure 4*D*. Fluorescence analysis of single HEK cells was done by manually selecting regions around each cell and separately a background region in open source ImageJ (version v1.48). Mean fluorescence intensity measurements were recorded for each region of interest (ROI). Background mean intensity was then used to background subtract from the cell mean intensity.

Fluorescence photo-bleaching in live *E. coli*

Fluorescence decay rates were measured for both CFP (111 mW, ex/em at 405/464-500 nm, 500 ms exposure) and merocyanine-bound Arch variants (32 mW ex/em at 727/770-840 nm, 250 ms exposure) allowing Arch decay rates to be presented relative to CFP. Relative measurements of photostability allow for correction of the 2D Gaussian laser intensity profile. Four clusters of ~40 cells were bleached for each variant; the images were cropped to the central 250x250 pixels, where the laser intensity profiles (the 405 and 727 nm lasers) were well-aligned. A mask was set for the first CFP-channel image to mitigate background (and applied to all subsequent images in the stack and to the corresponding Arch channel stack). A mask was not applied in the few cases where the pixel intensity histogram was unimodal. The mean pixel intensity was determined for each image. Fluorescence was normalized for protein absorption profile and measured laser intensity, and plotted over time. Time points represent the fluorescence after a given exposure time, where the camera and laser exposures have been synchronized so that the sample is only bleached while the camera is detecting. Plots (between 3 and 60s) were fit with a single exponential using the scipy.stats module in python. The [NIR fluorescence / CFP fluorescence] ratio of exponential decay rates was calculated for each spot of cells. The mean ratio for a given Arch variant (n = 4-5 spots) is given in Table 1.

HEK cell voltage-sensitive fluorescence imaging and electrophysiology

Imaging was performed concurrently with electrophysiology recordings of voltage-clamped cultured HEK cells using a Zeiss Axio Examiner.D1 microscope with a 20x 1.0 NA water immersion objective (Zeiss W Plan Apochromat × 20/1.0 DIC *D*=0.17 M27 75 mm). Voltage sensing fluorescence was excited with 650±13 nm LED light (Lumencor SPECTRAX light engine) with a 780 nm RazorEdge® ultrasteep long-pass edge filter (SEMROCK). Wild-type Arch and Mero-6 fluorescence was excited with 0.62 mW/mm^2 illumination intensity (20 mW power). The EGFP marker fluorescence was imaged with 485±25 nm LED light (Lumencor SPECTRAX light engine) with quad band 387/485/559/649 nm excitation filter, quad band 410/504/582/669 nm dichroic mirror and quad band 440/521/607/700 nm emission filter (all SEMROCK). Fluorescence frames were captured using an Andor Neo 5.5 sCMOS camera cooled to −30 °C at 250 Hz. All recordings were taken using Andor's Solis software.

Whole-cell patch-clamp recordings were done in cultured HEK cells 48 hours post transfection. Cells were continuously perfused with extracellular solution at room temperature (in mM: 140 NaCl, 5 KCl, 10 HEPES, 2 $MgCl_2$, 2 $CaCl_2$, 10 glucose; pH 7.35) while mounted on the microscope stage. Patch pipettes were fabricated from borosilicate capillary glass tubing (1B150-4; World Precision Instruments, Sarasota, FL) using a model P-2000 laser puller (Sutter Instruments) to resistances of 2–5 MΩ. Pipettes were filled with intracellular solution (in mM): 134 : gluconate, 5 EGTA, 10 HEPES, 2 $MgCl_2$, 0.5 $CaCl_2$, 3 ATP, 0.2 GTP. Whole-cell patch-clamp recordings were made using a Multiclamp 700B amplifier (Molecular Devices, Sunnyvale, CA), a Digidata 1440 digitizer (Molecular Devices), and a PC running pClamp (version 10.4) software (Molecular Devices) to generate current injection waveforms and to record voltage and current traces. Voltage-sensitivity patch recordings were done simultaneously with fluorescence imaging. For voltage sensitivity measurement cells were recorded in voltage clamp with a holding potential of −70 mV for 0.5 s and then 1 s voltage step was applied to +30 mV. To measure photocurrents of Arch variants, patch-clamp recordings were done with short light pulses. Photocurrents were measured with 485±25 nm, 590±25 nm and 650±13 nm light using LEDs at 8 mW/mm^2, 10 mW/mm^2, and 5

mW/mm^2 respectively (Lumencor SPECTRAX light engine). Photocurrents were also recoded with 730 nm light using a 730 nm laser (Changchun New Industries Tech. Co) at ~50 mW/mm^2. Photocurrents were recorded from cells in voltage clamp held at -50 mV with a 0.5 s light pulse.

HEK cell voltage-sensitive fluorescence data processing
Fluorescence analysis of patched cells was done by manually selecting regions around each cell and separately a background region in open source ImageJ. Mean intensity measurements were recorded for each region of interest (ROI) with background subtraction. Baseline fluorescence (F) was calculated for each cell by measuring the mean intensity during the -70 mV holding step. This was used to calculate ΔF/F for each cell over the time course of the experiment. The mean ΔF/F of 7 cells (Arch-WT) or 10 cells (Mero-6) was calculated for the time course of the experiment and plotted.

Synthesis and characterization of merocyanine retinal

General. Unless otherwise noted, all chemicals and reagents were obtained from commercial suppliers (Sigma-Aldrich, VWR, Alfa Aesar) and used without further purification. Unless otherwise noted, all reactions were performed under positive argon pressure. Reactions were monitored using thin layer chromatography (Merck 60 gel plates) using an UV-lamp for visualization. Silica gel chromatography purifications were carried out using AMD Silica Gel 60, 230-400 mesh. NMR spectra were obtained on a Bruker Prodigy 400 (400 MHz for ^{1}H; 101 MHz for ^{13}C NMR) in $CDCl_3$, and are referenced to the residual solvent peak. When appropriate, $CDCl_3$ was neutralized with sodium bicarbonate.

4-(1,3,3-trimethylindolin-2-ylidene)but-2-enenitrile (S-1). A dry round bottom flask, cooled under argon, was charged with NaH (60% dispersion in mineral oil, 0.36 g, 9 mmol). The flask was evacuated and filled with argon (3x), after which positive argon pressure was maintained on the flask. Anhydrous THF (22 mL) was added by syringe and the reaction mixture was cooled to 0 °C in an ice bath. Diethyl cyanomethylphosphonate (1.62 mL, 10 mmol, Sigma) was added dropwise and the reaction mixture was allowed to stir at 0 °C for 30 minutes. Following, 2-(1,3,3-trimethylindolin-2-ylidene)acetaldehyde (1.0 g, 5 mmol, Sigma) in anhydrous THF (10 mL) was added dropwise; the reaction was allowed to warm to room temperature and protected from light by covering the flask with aluminum foil. After 3 hours, the reaction was quenched by addition of brine. The water layer was extracted with diethyl ether; the combined organics were dried over sodium sulfate and concentrated *in vacuo*. The crude reaction mixture was purified by silica gel chromatography using 5:1 hexanes:ethyl acetate to provide the title compound as a light brown oil (1.09 g, 97% yield, 1:1 mixture of olefin isomers).

^{1}H NMR ($CDCl_3$, 400 MHz) for 1:1 mixture of isomers: δ 7.56 (dd, *J* = 15.2, 12.4 Hz, 0.5H), 7.36 (dd, *J* = 12.7, 10.5 Hz, 0.5H), 7.21 (tdd, *J* = 7.7, 2.9, 1.2 Hz, 1H), 7.18 – 7.14 (m, 1H), 6.94 (tdd, *J* = 7.5, 1.8, 1.0 Hz, 1H), 6.72 (t, *J* = 8.4 Hz, 1H), 5.71 (d, *J* = 12.7 Hz, 0.5H), 5.35 (d, *J* = 12.4 Hz, 0.5H), 4.90 (d, *J* = 15.2, 0.5H), 4.68 (d, *J* = 10.4 Hz, 0.5H), 3.22 (s, 1.5H), 3.16 (s, 1.5H), 1.56 (s, 3H), 1.56 (s, 3H).

4-(1,3,3-trimethylindolin-2-ylidene)but-2-enal (S-2). To a dry round bottom flask, cooled under argon, was added nitrile **S-1** (0.736 g, 3.28 mmol) and anhydrous dichloromethane (16.2 mL). A 1 M solution of DIBAL in cyclohexane (13.1 mL, 13.1 mmol) was added dropwise at room temperature. Reaction was protected from light by covering with aluminum foil and allowed to proceed at room temperature for 5 hours. The reaction mixture was diluted with ether, cooled to 0°C, and was quenched by adding 0.525 mL water, followed by 0.525 mL 1 M NaOH (aq), and 1.31 mL water. Mixture was warmed to room temperature and stirred for 15 min. Then, anhydrous magnesium sulfate was added and the heterogeneous mixture was stirred for an additional 15 min at room temperature. The crude mixture was filtered to remove salts and concentrated *in vacuo*. Purification was performed by silica gel chromatography using 3:2 hexanes:ethyl acetate to provide the title compound as a dark red solid (0.341 g, 45% yield, assigned as all *trans* isomer by NOESY).

^{1}H NMR ($CDCl_3$, 400 MHz): δ 9.46 (d, *J* = 8.3 Hz, 1H), 7.72 (dd, *J* = 14.2, 12.6 Hz, 1H), 7.26 – 7.17 (m, 2H), 6.98 (td, *J* = 7.5, 1.0 Hz, 1H), 6.76 (d, *J* = 7.8 Hz, 1H), 5.97 (dd, *J* = 14.2, 8.2 Hz, 1H), 5.55 (d, *J* = 12.6 Hz, 1H), 3.23 (s, 3H), 1.63 (s, 6H).

^{13}C NMR ($CDCl_3$, 101 MHz): δ 192.3, 165.5, 150.2, 144.0, 139.0, 128.0, 123.1, 121.7, 121.5, 107.2, 94.9, 46.7, 29.4, 28.4.

HRMS (FAB+): calculated for $C_{15}H_{17}NO$, $[M+H]^+$: 228.1388; found: 228.1365.

3-methyl-8-(1,3,3-trimethylindolin-2-ylidene)octa-2,4,6-trienenitrile (S-3). A dry round bottom flask, cooled under argon, was charged with NaH (60% dispersion in mineral oil, 0.127 g, 3.20 mmol). The flask was evacuated and filled with argon (3x), after which positive argon pressure was maintained on the flask. Anhydrous THF (7 mL) was added by syringe and the reaction mixture was cooled to 0 °C in an ice bath. Diethyl (3-cyano-2-methylallyl)phosphonate (mixture of isomers, 516 mg, 2.4 mmol, Sigma) was added dropwise at 0 °C. The reaction was allowed to warm to room temperature and stirred for 1 hour. The reaction vessel was protected from light by covering with foil for the remainder of the reaction. Following, aldehyde **S-2** (338 mg, 1.6 mmol) in anhydrous THF (3 mL) was added dropwise and reaction mixture stirred overnight. The reaction was quenched by addition of brine. The water layer was extracted with diethyl ether and combined organics were dried over magnesium sulfate and concentrated *in vacuo*. The crude reaction mixture was purified by silica gel chromatography using 5:1 hexanes:ethyl acetate to provide the title compound as an orange solid (0.380 g, 82% yield, 1:2 mixture of olefin isomers).

^{1}H NMR ($CDCl_3$, 400 MHz) for 1:2 mixture of isomers: δ 7.21 – 7.10 (m, 2H), 7.08 – 6.98 (m, 1H), 6.87 (tt, *J* = 7.4, 1.1 Hz, 1H), 6.80 – 6.61 (m, 2H), 6.20 – 6.02 (m, 2H), 5.43 – 5.34 (m, 1H), 5.06 (s, 0.66H), 4.93 (s, 0.34H), 3.15 (s, 1H), 3.13 (s, 2H), 2.20 (d, *J* = 0.9 Hz, 2H), 2.05 (d, *J* = 1.2 Hz, 1H), 1.59 (s, 6H).

(4*E*,6*E*)-3-methyl-8-((*E*)-1,3,3-trimethylindolin-2-ylidene)octa-2,4,6-trienal (2). To a dry round bottom flask, cooled under argon, was added nitrile **S-3** (0.38 g, 1.3 mmol) and anhydrous dichloromethane (8 mL). A 1 M solution of DIBAL in cyclohexane (5.3 mL, 5.3 mmol) was added dropwise at room temperature. Reaction was protected from light by covering with aluminum foil and allowed to proceed at room temperature for 5 hours. For workup, the reaction mixture was diluted with ether, cooled to 0°C, and was quenched by adding 0.211 mL water, followed by 0.264 mL 3 M NaOH (aq), and 0.528 mL water. Mixture was warmed to room temperature and stirred for 15 min. Then, anhydrous magnesium sulfate was added and the heterogenous mixture was stirred for an additional 15 min at room temperature. The crude mixture was filtered to remove salts and concentrated *in vacuo*. Purification was performed by silica gel chromatography using 9:1 hexanes: ethyl acetate to provide the title compound as a dark red solid (0.214 g, 55% yield, assigned as 3:1 trans/cis mixture of olefin isomers by NOESY).

^{1}H NMR ($CDCl_3$, 400 MHz) for 3:1 trans/cis mixture of isomers: δ 10.18 (d, *J* = 8.2 Hz, 0.25H), 10.06 (d, *J* = 8.4 Hz, 0.75H), 7.22 – 7.11 (m, 2H), 7.06 (dd, *J* = 14.1, 12.2 Hz, 1H), 6.97 – 6.83 (m, 2H), 6.64 (d, *J* = 7.8 Hz, 1H), 6.26 – 6.08 (m, 2H), 5.92 (d, *J* = 8.4 Hz, 0.75H), 5.75 (d, *J* = 8.1 Hz, 0.25H), 5.40 (d, *J* = 12.1 Hz, 1H), 3.14 (s, 3H), 2.31 (s, 2.25H), 2.13 (s, 0.75H), 1.60 (s, 6H)

^{13}C NMR ($CDCl_3$, 101 MHz) for 3:1 trans/cis mixture of isomers: δ 190.8, 189.8, 159.4, 155.8, 155.6, 144.8, 139.3, 138.9, 138.5, 135.5, 129.6, 127.9, 127.3, 125.7, 124.3, 121.6, 120.1, 106.3, 96.7, 45.8, 29.2, 28.4, 21.3, 13.1

HRMS (FAB+): calculated for $C_{20}H_{23}NO$, $[M+H]^+$: 294.1858; found: 294.1844.

Synthesis and characterization of merocyanine-Schiff base compound

(4*E*,6*E*)-*N*-butyl-3-methyl-8-((*E*)-1,3,3-trimethylindolin-2-ylidene)octa-2,4,6-trien-1-imine (S-4). The title compound was synthesized following the general procedure of G. Bassolino *et al*., from merocyanine retinal 2 (Bassolino et al., 2014). Briefly, a 25-mL round bottom flask was charged with 850 mg molecular sieves 3Å, which were activated by flame drying under vacuum. The flask was cooled to 0 °C under argon. Merocyanine retinal 2 (18 mg, 61 μmol) and anhydrous methanol (9 mL) were added to the flask, and allowed to cool to 0 °C. Following, *n*-butylamine was added dropwise (94 μL, 952 μmol). The flask was wrapped in foil to protect from light and the reaction was allowed to proceed for 70 minutes at 0 °C. The crude reaction mixture was filtered over a pad of Celite® 545; the Celite pad was washed with dichloromethane. The solvent and excess *n*-butylamine were removed by rotary evaporator under vacuum with the water bath of the rotary evaporator at or below 25 °C. The compound was protected from light during the entire work-up process. No purification was performed; the crude product was obtained as a dark red oil (20.4 mg, 96% yield). Crude ^{1}H NMR ($CDCl_3$, 400 MHz) shows two distinct imine proton

peaks in a 3:1 ratio (δ 8.28 (dt, J = 9.6, 1.4 Hz, 0.75 H) and 8.44 (dt, J = 9.7, 1.4 Hz, 0.25 H), respectively), giving strong evidence that the title Schiff-base compound was formed. Note: impurities were observed in the ^{1}H NMR of the crude Schiff base product.

Supplemental References

Asson-Batres, M.A., Smith, W.B., and Clark, G. (2009). Retinoic acid is present in the postnatal rat olfactory organ and persists in vitamin A--depleted neural tissue. J Nutr *139*, 1067-1072.

Bassolino, G., Sovdat, T., Liebel, M., Schnedermann, C., Odell, B., Claridge, T.D., Kukura, P., and Fletcher, S.P. (2014). Synthetic control of retinal photochemistry and photophysics in solution. J Am Chem Soc *136*, 2650-2658.

Edelstein, A., Amodaj, N., Hoover, K., Vale, R., and Stuurman, N. (2010). Computer control of microscopes using microManager. Curr Protoc Mol Biol *Chapter 14*, Unit14 20.

Muenzner, M., Tuvia, N., Deutschmann, C., Witte, N., Tolkachov, A., Valai, A., Henze, A., Sander, L.E., Raila, J., and Schupp, M. (2013). Retinol-binding protein 4 and its membrane receptor STRA6 control adipogenesis by regulating cellular retinoid homeostasis and retinoic acid receptor alpha activity. Mol Cell Biol *33*, 4068-4082.